



Experimental and numerical dynamic analysis of a live tree stem impacted by a Charpy pendulum

D. Bertrand^{a,*}, F. Bourrier^b, I. Olmedo^{a,b}, M. Brun^a, F. Berger^b, A. Limam^a

^a INSA Lyon/LGCIE (Laboratoire de Génie Civil et Ingénierie Environnementale), Bâtiment Coulomb 20, Avenue A. Einstein 69621, Villeurbanne cedex, France

^b Irstea Grenoble/EMGR (Ecosystèmes montagnards) 2, rue de la Papeterie – domaine universitaire BP 76, 38402 St-Martin-d'Hères Cedex, France

ARTICLE INFO

Article history:

Received 24 October 2012

Received in revised form 15 January 2013

Available online 19 February 2013

Keywords:

Rockfalls

Natural hazards

Live tree stem

Impact dynamics

FEM non linear computations

Experimental impact tests

Calibration and validation

ABSTRACT

In recent years, the forest has been used as a protective structure to reduce rockfall propagation. When a rock propagates down a forested slope, it hits trees and these interactions modify its trajectory. This paper focuses on the dynamic behavior of small-diameter live trees impacted by a rock. To better understand the protective effect of forests against rockfalls, a finite element (FE) model of a live stem subjected to a local dynamic loading is proposed. Large displacements and material nonlinearities are taken into account. The numerical simulations are calibrated based on laboratory tests (free oscillation tests and impact tests). The displacement field measured by a high-speed camera is correctly reproduced by the FE model for both kinds of tests. For impact tests, the analysis of the impactor–stem interaction identified three main regimes of the stem's response (quasi-static/intermediate/impulsive). These depend on the impactor's and stem's mechanical and geometrical features (relative mass and stiffness). Finally, we attempt to predict the regime response of the stem as a function of its diameter and the impactor mass.

© 2013 Elsevier Ltd. All rights reserved.

1. Introduction

The propagation of a rock along a slope depends on many factors related to rock and slope properties. Most of the key scientific points lie in the description of the interaction between the block and the potential obstacles during its propagation. Over the last three decades, many models have been proposed (Volkwein et al., 2011) for the interaction with the soil surface.

The use of rockfall protection forests is becoming a common practice (Perret et al., 2004; Dorren, 2006; Cameron and Peloso, 2009), and the assessment of the protective role of standing trees using rockfall simulation models is a new challenge. Much research has been undertaken to assess the energy transfers during the impact of rocks on standing trees. These energy transfers are closely related to the strength of live trees, which can be estimated from field experiments (Stokes et al., 2005; Ruel et al., 2010; Urata et al., 2012) or from the results of other research fields such as tree resistance to wind (Wilson, 2004; Hu et al. (2008)). Tree–rock interactions have already been studied for specific configurations (Quétel, 2005; Jonsson, 2007; Lundstrom et al., 2007). However, depending on the relative sizes of rocks and trees the impact can be completely different. Quantifying the energy transfers in different configurations is therefore of specific interest. Many authors

have studied wood using FE models (Mackerle, 2005). Dynamic analysis is often carried out considering elastic mechanical behavior (Sellier et al., 2006; Hu et al., 2008). Modeling the dynamics of live tree stems requires choosing between different numerical approaches depending on their relevancy and computational efficiency, especially if nonlinearities are taken into account.

This paper aims at identifying the key processes managing the impact of a rock on a small-diameter live tree stem. Therefore, an efficient (simple but realistic) FE model of a live stem subjected to dynamic loadings is investigated. Rockfall simulations are usually conducted in a stochastic framework which involves many simulations to be done. Thus, the objective is to develop a FE model able to describe the physics of the interaction and efficient in terms of CPU time. For that purpose, laboratory impact experiments were used to calibrate and validate the FE model. Finally, the key processes managing the impact have been highlighted using numerical investigations.

2. Materials and methods

2.1. FE model assumptions

During an impact, several nonlinear phenomena develop. In the case presented, large stem displacements and rotations are observed and taken into account. Material nonlinearities can appear inside the stem and should be described by an *ad hoc* rheological model.

* Corresponding author. Tel.: +33 472437294.

E-mail address: david.bertrand@insa-lyon.fr (D. Bertrand).

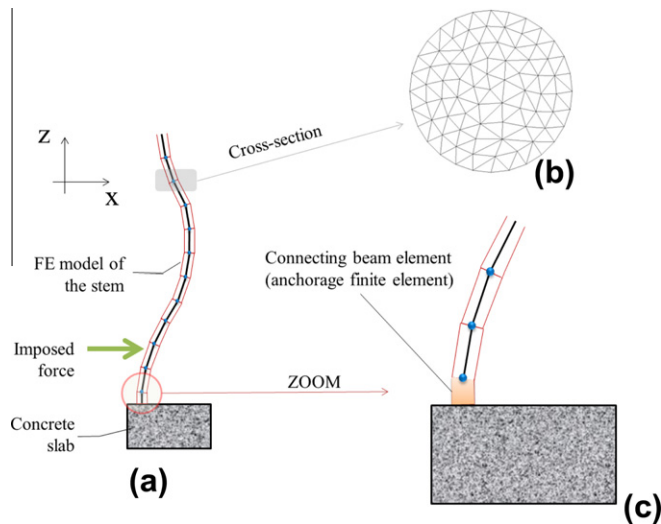


Fig. 1. FE model of the stem. Boundary conditions and longitudinal meshing (a), meshing of the cross-section (b) and anchorage stiffness of the foot of the stem (anchorage element) (c).

Because mechanical tests generally focus on defect-free specimens (Mindess and Madsen, 1986; Reid and Peng (1997); Salmi et al., 2012), little information is available in the literature on the macroscopic mechanical behavior of live trees under dynamic loadings.

For the sake of simplicity, the following assumptions are proposed. The mechanical response in tension and compression of living beech wood (*Fagus sylvatica* L.) is assumed to follow the stress/strain curve proposed by Trouy-Triboulot and Triboulot (2008), which is similar to rheology used for lumber (Adalian and Morlier, 2002; DaSilva and Kyriakides, 2007; Oudjene and Khelifa, 2009; Neumann et al., 2011). The behavior law implemented in the FE model takes into account the dissymmetry of the mechanical response in tension and compression regimes. The longitudinal behavior of live wood in compression is described by an elastoplastic behavior law with strain hardening and an elastic brittle model in tension.

For impact tests, the loading of the stem originates in the interaction between two colliding bodies. Handling contact nonlinearities by FE models is a tricky problem involving important algorithmic developments. In addition, the contact law's parameters are not always easy to calibrate. To overcome these aspects and stay as close as possible to the physics of the interaction, an imposed force has been applied to the stem at the impacting point.

Given the fibrous nature of wood, multifiber finite elements were used (Guedes et al., 2000) to simulate the beam's bending accounting each fiber. Along the longitudinal axis of the stem, segments with two nodes were used and spatial discretization of the cross-section was performed with three-nodes triangle elements (Fig. 1a–b). As shearing can be substantial close to the impacted zone, Timoshenko beam theory was considered (Timoshenko and Krieger, 1959).

2.2. Laboratory experiments

Winching tests (free oscillation tests) and impact tests were performed in laboratory conditions. Three winching tests and four impacts were selected to calibrate and validate the FE model.

2.2.1. Stem properties

The stems were selected in accordance with typical tree populations encountered in rockfall protection forests and their diameters were chosen to obtain significant displacements and

potential failures under the experimental loadings applied (low impact energy). Small-diameter trees were collected in a coppice stand near Grenoble (France). The stems collected correspond to young trees composed of primarily juvenile wood, with highly variable material properties. As the stem properties strongly depend on the growing conditions, age, and genetics of the trees, the quantitative results obtained in the followings are only valid for trees with similar properties as those of the selected trees. However, the modeling approach can be extended to other type of trees. The experiments were conducted exclusively on beech stems considering that beech is the most common tree species in rockfall protection forests with fir (Dorren, 2006).

Wood rheology is strongly influenced by its moisture content. However, over the fiber saturation point, mechanical property changes are limited (Risbrudt and Ritter, 2010). Characterizing of the mechanical properties of young trees therefore requires experimental tests representing *in situ* conditions: freshly cut stems were subjected to the dynamic tests.

After removing the branches, the specimens tested were weighed and the diameters were measured at regular intervals along the stems. To maintain the mechanical and physical properties of live wood, the experimental tests were done a maximum 3 days after cutting. The foot of the stems was immersed in a barrel filled with water to limit the evaporation of the water contained in the wood fibers.

2.2.2. Displacement measurements

High-speed cameras were used to measure the displacement field of the stem and the impactor (Fig. 2). Measurements were taken at the scale of the entire stem to capture the stem's overall motion (210 fps) and locally at the impact point (in the impact tests, 600 fps). An image-processing algorithm was used to follow trajectories of several points (white marks) on the stem.

Because of the optical aberrations of the objective lens, objects far from the optical axis of the camera are deformed. By taking a picture of a pattern whose dimensions are known, the correction factor to be applied to the image was determined. This step provided a corrected image and reduced the measurement error on the displacements.

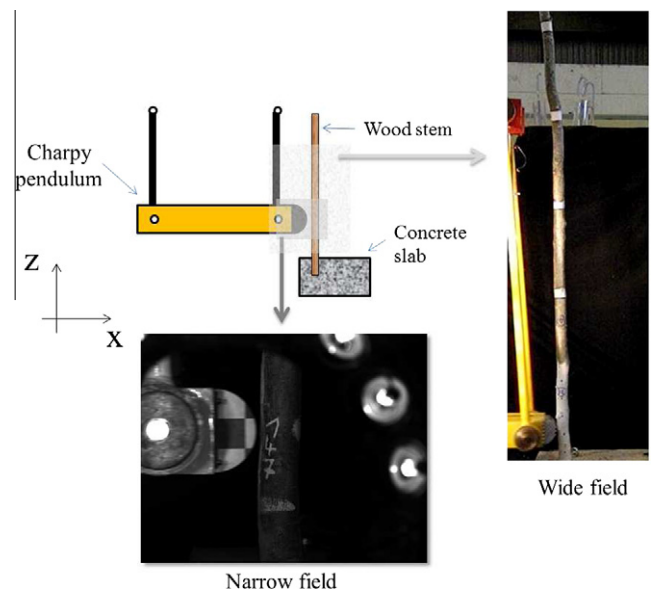


Fig. 2. Optical measurements (wide, stem scale; narrow fields, contact point scale) of the stem's displacement field impacted by the ram.

2.2.3. Winching tests (free oscillation tests)

Winching tests assess the mechanical properties of *in situ* standing trees (Jonsson, 2007). In this study, cut trees were subjected to winching tests to characterize the dynamic Young modulus (E_b) and damping (ξ) of the tested stems. The feet of the stems were cemented in a fixed support to remove the effect of the root-earth system.

The test consists in imposing an initial displacement at the top of the stem (P4) to bend it to a given initial position (Fig. 3). Then the sudden release of the top of the stem generates the oscillation of the stem around its vertical equilibrium position. White marks are used to measure the time evolution of the trajectories of specific points P3 and P4.

2.2.4. Impact tests

The impact tests were performed using an impactor that strikes the specimen, usually called Charpy pendulum (ASTM, 2010). The Charpy pendulum is a parallelepiped linked to a fixed steel frame by four steel bars (Fig. 4). The length of each bar is $L_b = 1.75$ m. The bars can rotate around fixed points, ensuring a circular translational motion of the ram generating a uniform

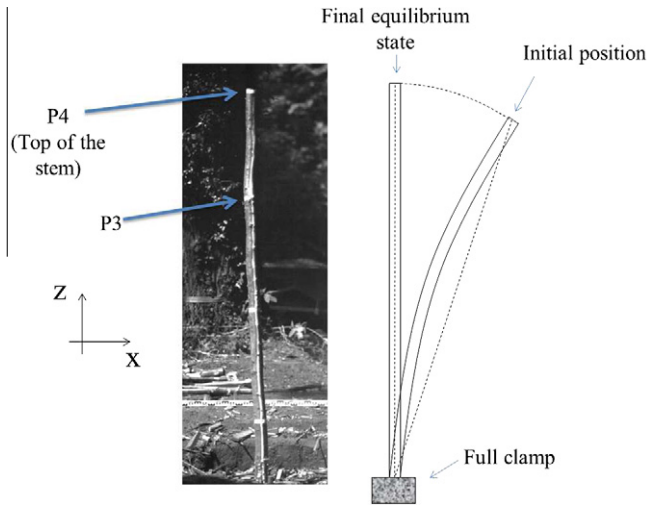


Fig. 3. Experimental protocol of the winching tests (free oscillation tests).

acceleration field. The mass of the pendulum is 93.3 kg and each bar weighs 36.6 kg.

A concrete slab on the floor maintains the stems in a vertical position. The stem is placed in a hole into which cement is poured to fix the motion of its foot. Once the cement setting is set (about 2 days, with rapid hardening cement), the impact test is ready. After the test, the cement is removed from the hole and another test can be carried out.

2.3. FE modeling of the experiment

2.3.1. Boundary conditions

As the boundary conditions applied in the experiments (rigid clamped support and tree crown cut) were different from natural conditions, the distribution of the strains and stresses along the stem, as well as the location of the maximum acting moment on the stem, potentially differed from the conditions observed for rock impacts in the field.

For the experimental winching tests, the anchorage was not damaged during the test and was therefore modeled as a full clamp.

On the other hand, during the impact tests and especially for large stem diameter (>60 mm), the rotation of the foot of the stem generated a local crushing of the cement, implying the loss of the full clamp condition. To account for this phenomenon in the FE model, a single beam finite element (so-called anchorage element) was inserted between the rigid support and the stem (Fig. 1c). Therefore, several Young modulus values of the anchorage element were defined depending on the displacement of the stem. Three main phases can be identified. First, the initial rotation of the foot's stem crushes of the cement (phase 1) until the compaction state of the cement induced a substantial increase in stiffness (phase 2). Then the flexural waves returned back to the fixation point and unload the cement (phase 3). Since during the first phase the cement was totally crushed, the stiffness was very low during phase 3. Consequently, the complete definition of the elastic properties of the anchorage element requires calibrating three parameters representing the evolution of the anchorage rotational stiffness: $EyCL1$, $EyCL2$, and $EyCL3$.

2.3.2. Stem loading modeling

To model the winching test loading conditions, a constant force was applied in the direction of the rope until the top of the stem

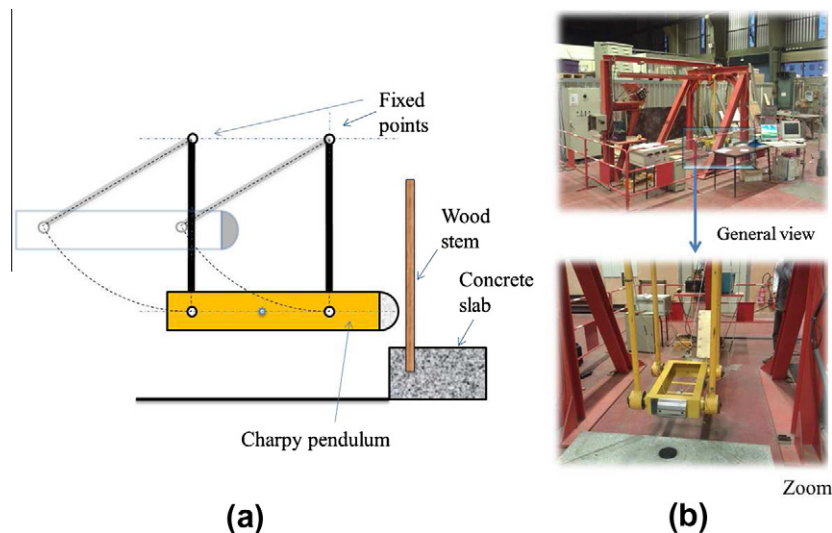


Fig. 4. Charpy pendulum scheme (a) and impacting device photographs (b).

reached the initial experimental position and the loading force was set at zero to reproduce the sudden cut of the rope.

For the impact test, the load was applied by a contact force from the ram action. The computational time can be significantly reduced (Pashah et al., 2008) if the contact force is modeled as an external force. In this case, the loading was applied along the horizontal direction (along the x -axis) at the contact point and its time evolution was unknown. Since no accurate experimental data were available on the load's shape over time, the time evolution of the force was postulated.

The shape of the contact force over time is strongly related to the impactor-stem interaction. The influence of the mechanical system flexibility to low-velocity impacts has been studied by many authors (Goldsmith, 1960; Biggs, 1964; Schwiager, 1970; Mittal, 1989; Abrate, 2011). Three typical impact situations exist: the quasi-static (or global) regime, impulsive (or local) regime, and intermediate regime (Christoforou and Yigit, 1998). The first one corresponds to impact situations where the structure's response is global and static in nature. In the opposite case, the impact force history can be considered an impulsive loading and the structure responses as a vibrating system (local loading). The intermediate regime is a combination of these effects.

For a transverse impact on flexible structures such as beams, the nature of the impact response depends on the masses of the colliding bodies, the location of the impact in relation to boundaries and finally the deformability of the contact region in comparison to the structural stiffness (Stronge, 2000). These three factors determine the number of vibration modes involved in the structure's response. The reflected waves from the boundary through the beam interact with the impactor during the contact phase and thus have a significant influence on the duration, magnitude and shape of the contact force.

Specific times of the structural response can be assessed by the modal oscillation periods. Considering the mean values of the stems studied, the first four modal periods were assessed using a modal analysis. For a stem 81 mm in diameter, weighing 15 kg, and 2.75 m in high, with a Young modulus of 14000 MPa, they equal $t_{f1} = 0.25$, $t_{f2} = 0.028$ and $t_{f3} = 0.012$ s. From an experimental point of view, the mean contact duration is about 0.05 s. These times are on the same order of magnitude, which suggests that the structure's response cannot be simplified to an asymptotic solution. The interaction between the pendulum and stem predominates.

In the intermediate regime, the shape of the contact force exhibits a typical multipeak shape over time. For instance, Miyamoto et al. (1991) measured the impact force developed during the collision of a pendulum and a multimass system (cubic metal bodies linked by rubber pads acting as springs and dashpots). The interaction between the pendulum and the impacted system developed a double-peak shape of the impact force–time relation.

To propose an appropriate loading force over time to apply to the stem, the horizontal displacement of the pendulum was measured to provide a polynomial fit of the curve. The derivation of the polynomial fit gives the qualitative shape of the pendulum's acceleration and thus the loading force shape (Fig. 5). Although the double derivation increases the measurement uncertainties implying that the results are only qualitative, a typical double-peaked curve was observed and used to load the stem over time.

2.3.3. Loading force for impact tests

The time evolution of the contact force during the impact is assumed to exhibit a typical double-peaked shape. Consequently, the curve was defined as the combination of two Beta laws. The force signal can be written as $\forall t' \in [0, 1]$ with $t' = t/t_c$:

$$F(t') = F_{max} \frac{t'^{\alpha_1-1} (1-t')^{\beta_1-1} + t'^{\alpha_2-1} (1-t')^{\beta_2-1}}{\int_0^1 (u^{\alpha_1-1} (1-u)^{\beta_1-1} + u^{\alpha_2-1} (1-u)^{\beta_2-1}) du} \quad (1)$$

and, for $\forall t > t_c$, $F(t) = 0$. t_c is the contact duration and F_{max} is the maximum force. The parameters α_1 , β_1 , α_2 and β_2 shape the curve.

The experimental parameters used for calibration are the impulse \mathbb{I} applied on the stem and the contact duration t_c .

The momentum variation of the pendulum equals the impulse \mathbb{I} applied to the stem. The following equation allows calculating \mathbb{I} from the apparatus impacting masses (pendulum and supporting bars) and the relative velocities of the pendulum before (v_{G1}^{av}) and after (v_{G1}^{ap}) the impact.

$$\mathbb{I} = \left(m_1 + \frac{4}{3}m_2\right)(v_{G1}^{ap} - v_{G1}^{av}) = \left(m_1 + \frac{4}{3}m_2\right)\Delta v \quad (2)$$

where m_1 is the pendulum mass and m_2 is the mass of one of the pendulum's bars.

The impulse \mathbb{I} is also related to the force signal as follows:

$$\mathbb{I} = \int_0^{t_c} F(t) dt \quad (3)$$

The identification of these two relationships knowing the measured contact duration t_c , assesses the parameters characterizing the force evolution: α_1 , β_1 , α_2 , β_2 and F_{max} .

3. Results

3.1. FE model calibration

3.1.1. Winning tests

To assess the magnitude order of the Young modulus and damping coefficient for the beech stems, three winning tests were performed. The k th winning test is called $WiTe^{(k)}$. All the stems were 3 m long and the Poisson ratio (ν) was set at 0.35. This is an average value found in the literature (Risbrudt and Ritter,

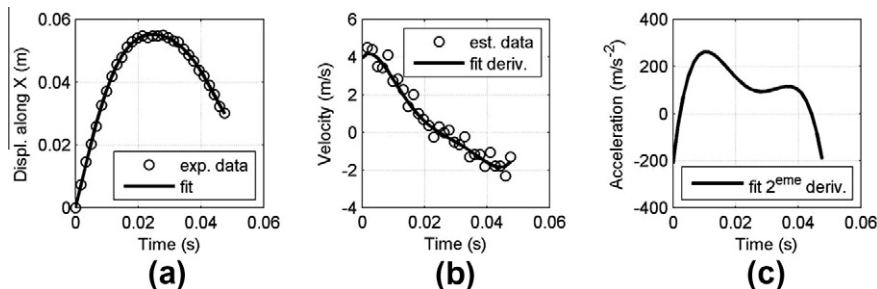


Fig. 5. Measurements taken at the contact point for the test $ImTe^{(2HE)}$. Time vs. horizontal displacement (along the x -axis) of the impactor during the contact is depicted (a). The dots represent the experimental points and the continuous line is its polynomial fit. The velocity of the impactor (b) is obtained by the derivation of the fitted curve and the dots are the experimental velocity estimations from the experimental displacements. Finally, the pendulum's acceleration shape is assessed by the double derivation of the fit of the displacement (c).

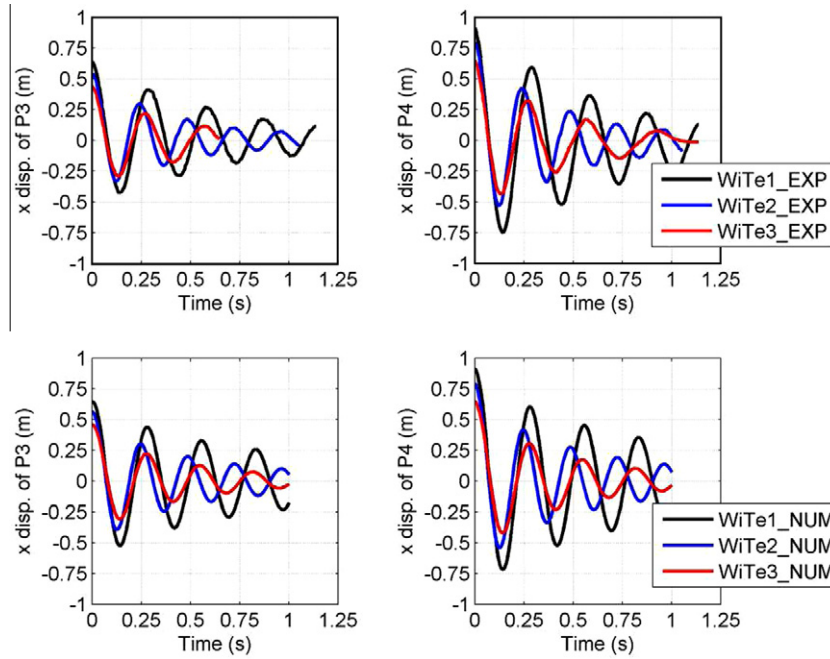


Fig. 6. Time vs. the horizontal positions (along the x-axis) of the white marks P3 (a-c) and P4 (b-d). Comparison between the experimental measurements (a-b) and FE model results (c,d) after calibration of E_b and ξ . The final coordinates of P3 (resp. P4) are $x_3 = 0, z_3 = 2.25$ m (resp. $x_4 = 0, z_4 = 3$ m).

2010). The effects of ν on the kinematics are very low because the stem's response is mainly controlled by bending effects. The time evolution of the horizontal positions of P3 and P4 are depicted for the three stems tested (Fig. 6a-b). After calibration, very good

agreement is shown between the simulation results and the experimental measurements. The calibration data are summarized in Table 1.

3.1.2. Impact tests

FE model calibration from the experimental data consists in two steps. First, the elastic parameters were calibrated using low impact energy (LE - 728 J), assuming that the stem's response remained elastic. Second, the same elastic parameters were used for an impact on the same stem at high energy (HE - 1355 J). There, the potential damage can be observed at the foot of the stem.

The model's calibration is presented for two stems ($ImTe^{(kj)}$ with k the number of the stem and $j = LE, HE$ the impact energy involved during the test). The stem's characteristics are listed in Table 1. Thus, for each stem, two successive experimental impact

Table 1

Calibrated (**in bold**) and measured parameters (*in italics*) used in the FE simulations of winching and impact tests.

Stem parameters	Winching tests			Impact tests	
	<i>WiTe⁽¹⁾</i>	<i>WiTe⁽²⁾</i>	<i>WiTe⁽³⁾</i>	<i>ImTe⁽¹⁾</i>	<i>ImTe⁽²⁾</i>
Length (m)	3	3	3	2.84	2.75
Diameter (mm)	76.3	64.7	75.6	52	81
Mass (kg)	14.6	9	14.7	6.2	14.55
Young modulus (MPa)	10,000	16,000	11,000	15,000	14,000
Damping (%)	3	5	8	0.5	6.5

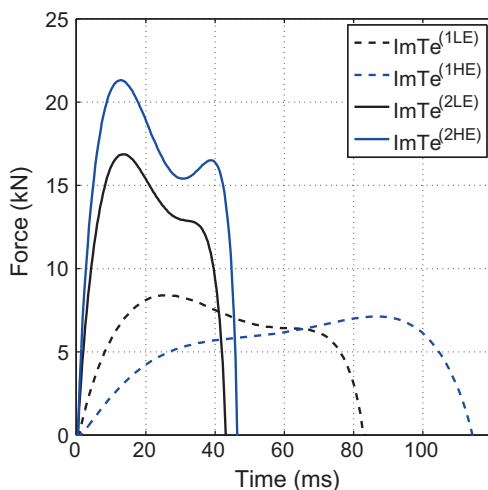


Fig. 7. Time vs. the force applied to the stems for all impact tests ($ImTe^{(1LE)}$, $ImTe^{(1HE)}$, $ImTe^{(2LE)}$ and $ImTe^{(2HE)}$).

Table 2

Calibrated (**in bold**) and measured parameters (*in italics*) used in the simulations of low- and high-energy impacts. t_{ph1} (resp. t_{ph2}) corresponds to the transition time between the first phase (resp. second) and the second (resp. third) phase. t_c (resp. t_c^e) is the measured (resp. estimated) contact duration.

Stem parameters	Impact tests			
	<i>ImTe^(1LE)</i>	<i>ImTe^(2LE)</i>	<i>ImTe^(1HE)</i>	<i>ImTe^(2HE)</i>
Velocity before impact (m/s)	3.07	3.21	4.28	4.42
Velocity after impact (m/s)	−0.58	−0.59	0.16	−0.82
Contact time (s)	0.082	0.043	0.113	0.046
Impulse (Ns)	520	543	587	747
EyCL1 (MPa)	400	725	1.1	550
EyCL2 (MPa)	4000	2750	300	42000
EyCL3 (MPa)	72	–	–	–
t_c (ms)	82	43	113	46
t_c^e (ms)	77	32	77	32
t_{ph1} (s)	$1/3 \times t_c$	$3/5 \times t_c$	$1/2 \times t_c$	$2/3 \times t_c$
t_{ph2} (s)	$2/3 \times t_c$	–	–	–
α_1 (–)	1.8	1.8	4.5	1.7
β_1 (–)	5.8	5.8	1.9	5.8
α_2 (–)	3.2	3.2	2.2	3.3
β_2 (–)	1.9	1.9	4.1	1.8
F_{max} (kN)	8.40	16.88	7.12	21.33

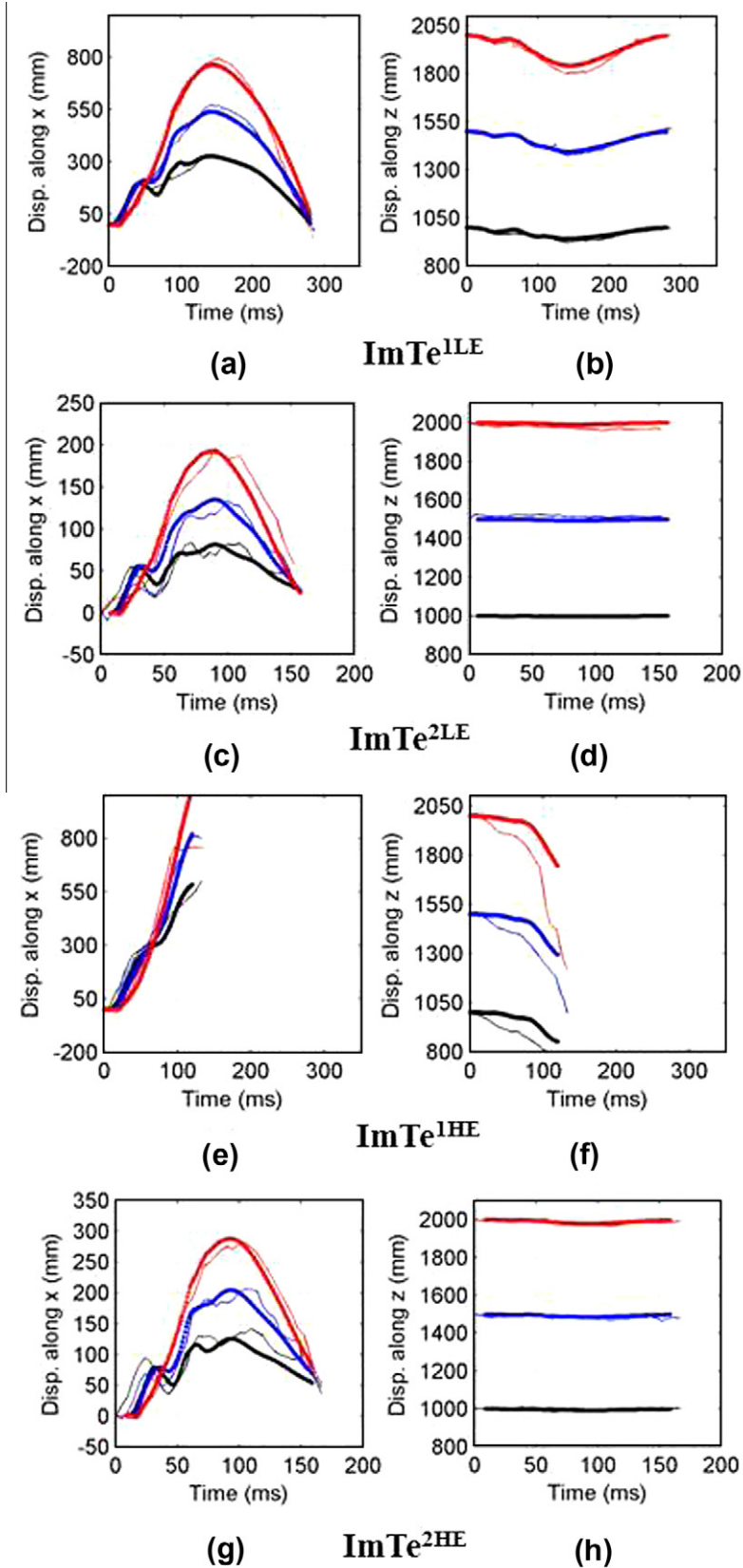


Fig. 8. Comparison of numerical and experimental results of the impact tests. The displacement along the x -axis (a–c–e–g) and along the z -axis ((b–d–f–h) of the three white marks are depicted as a function of time. The measured (resp. simulated) displacements are drawn by thin lines (resp. thick lines).

tests were carried out. The stems were impacted at 28 cm from the boundary condition. The assumed impact loads are depicted in Fig. 7. Four simulations were calibrated on these experimental

data. The simulation parameters are summarized in Tables 1 and 2 for both impacted stems. The elastic limit in tension and compression were set at 100 MPa and 50 MPa, respectively.

3.1.2.1. Low-energy impact. Fig. 8a-b-c-d compares experimental data and FE simulations for low-impact energy (728 J). The impulses were similar but the contact duration of $ImTe^{(2LE)}$ was half the contact duration of $ImTe^{(1LE)}$, inducing a lower maximal force. These differences also came from the bending stiffness of the stems. The stem's $ImTe^{(1)}$ diameter was only half $ImTe^{(2)}$. The Young moduli calibrated were also very similar to those found for the winching tests. Finally, the results show that the rotational stiffness of the anchorage strongly modified the stem's overall response. A decrease in this stiffness induced damping of the flexural waves, which reduced the overall kinematics.

3.1.2.2. High-energy impact. For high impact energy, the results are presented in Fig. 8e-h. In $ImTe^{(2HE)}$, the potential damage developed during the first impact test seems to have a limited influence on the stem's response to a second impact and thus it can be assumed the stem's response is mostly elastic.

The $ImTe^{(1HE)}$ test, the stem broke and the model results do not agree with the experimental data even if the rheology accounts for the nonlinearities of the material. From an experimental point of view, the instant of the stem's rupture is not the same, implying a completely different kinematics after the rupture point.

To assess the influence of the material nonlinearities on the stem's dynamic response, simulations were performed using a purely elastic behavior law. For the $ImTe^{(1HE)}$, $ImTe^{(2LE)}$ and $ImTe^{(2HE)}$ impacts tests, the results were quite similar. The difference in terms of maximum displacements was less than 6%. However, for $ImTe^{(1HE)}$, the rupture of the stem's foot could not be reproduced, implying a completely different displacement field.

3.1.2.3. Discussion on the calibration results. For each stem, the comparison of the calibrated parameters led to similar wood properties at low and high energies.

The rotational stiffness of the anchorage and the damping coefficients can be seen as a pair of parameters strongly influencing the structure's deformation and the vibration modes governing its motion. For quasi-rigid anchorage and low damping coefficients, high-frequency modes developed. The differences between low-energy and high-energy impacts were, for stem 1, a decrease in the anchorage rotational stiffness and a slight increase in the damping coefficient. For stem 2, the same tendency was observed and the increase in the damping coefficient is more pronounced, leading to a smaller contribution of the high-frequency modes. This is physically consistent because between the two energy levels, the anchorage and the stem were damaged due to local breakage and cracks that dissipate energy.

For the first stem ($ImTe^{(1)}$), impact forces did not have the same shape for low- (LE) and high- (HE) impact energies (Fig. 7) because the stem breakage occurrence modifies the interaction between the ram and the stem.

In the second stem ($ImTe^{(2)}$), the loading force shapes are qualitatively the same for low (LE) and high (HE) energies. The first peak of the force is similarly marked for both impact energies. The instant of the peak can be correlated with the stem bending stiffness and the mass ratio between the stem and the ram. Its intensity is related to the ram velocity before impact, which explains the magnitude differences between low and high energy. The second peak, which can be seen as a second loading of the stem after its first elastic round-trip, is more pronounced for high energy: as the initial velocity of the ram is higher, more energy was left to the stem.

3.2. Key parameters managing the interaction

This study has attempted to identify the type of interaction (impulsive, quasi-static, or intermediate) developed during the impact between the impactor and the stem. Two parametrical studies

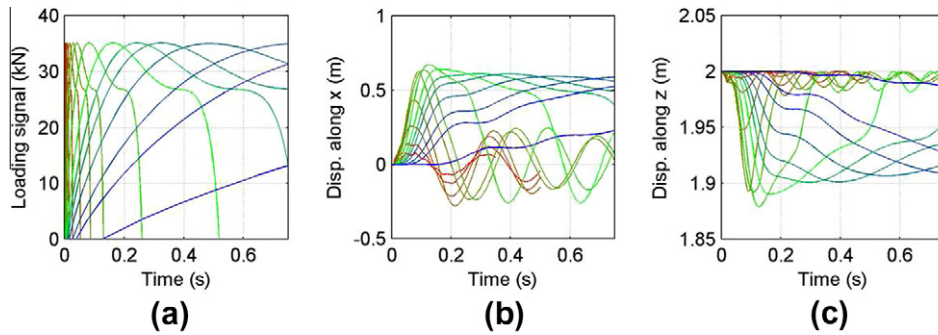


Fig. 9. FE simulations highlighting the influence of the loading time on the stem's dynamic response. The peak force was kept constant (35 kN). Time vs. the imposed force (a), the displacement along the x-axis (b) and along the z-axis (c) of the top of the stem for corresponding loading time values (color correspondence).

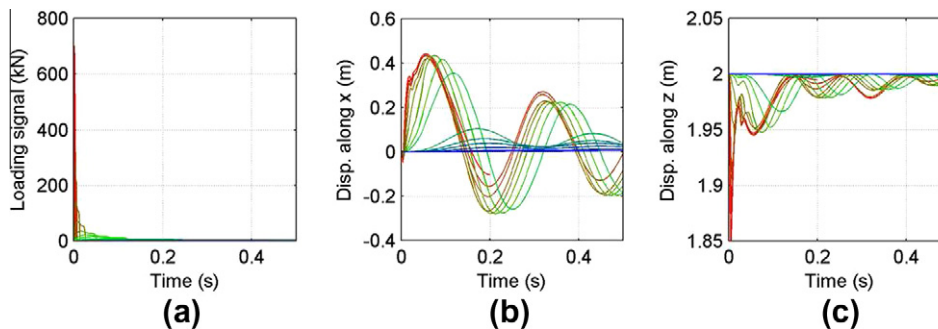


Fig. 10. FE simulations highlighting the influence of the loading time on the stem's dynamic response. The impulse was kept constant (1360 Ns). Time vs. the loading signal (a), the displacement along the x-axis (b) and displacement along the z-axis (c) of the top of the stem for corresponding loading time values (color correspondence).

were conducted considering the geometrical and mechanical features of the $ImTe^{(2)}$ stem.

First, for a given peak force (35 kN), the loading duration was varied inducing the change in the applied impulse (Fig. 9). The range explored was $170 \text{ Ns} < I < 340 \text{ kNs}$. Second, for a given im-

pulse value ($I = 1360 \text{ Ns}$), simulations were performed for different loading durations (Fig. 10). The maximum force (F_{max}) ranged from 467 N to 702 kN. For both parametrical studies, the range explored in terms of loading time was $t_{f1}/100 < t_c < 50 t_{f1}$, where t_{f1} is the first natural frequency of the stem considered.

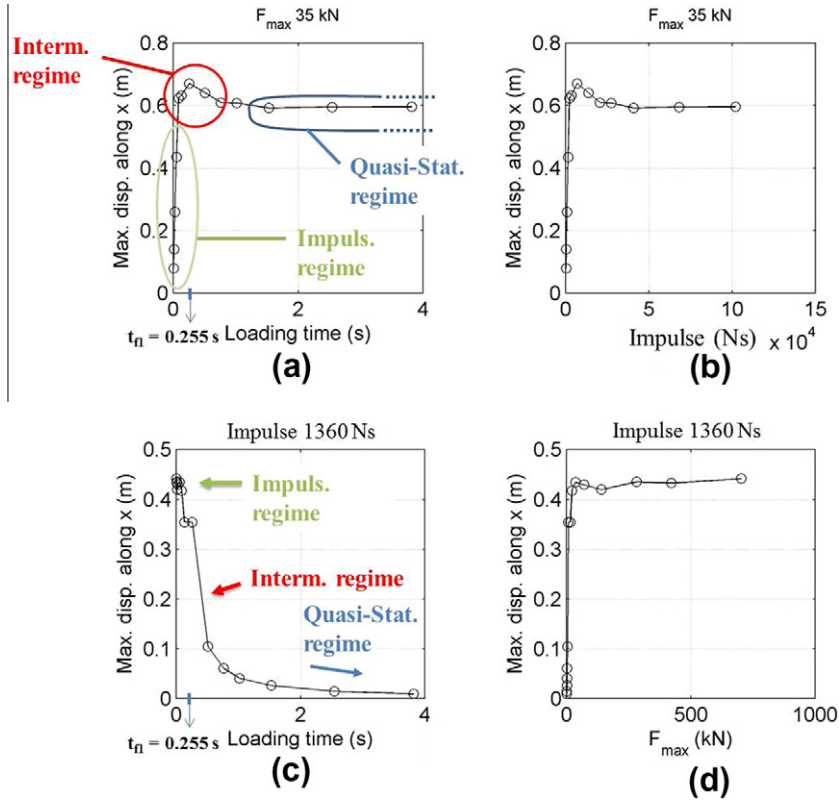


Fig. 11. Maximum displacements of the top of the stem as a function of the loading time for $F_{max} = 35 \text{ kN}$ (a) and $I = 1360 \text{ Ns}$ (c). The curve (b) (resp. (d)) represents the maximum displacement as a function of I (resp. F_{max}).

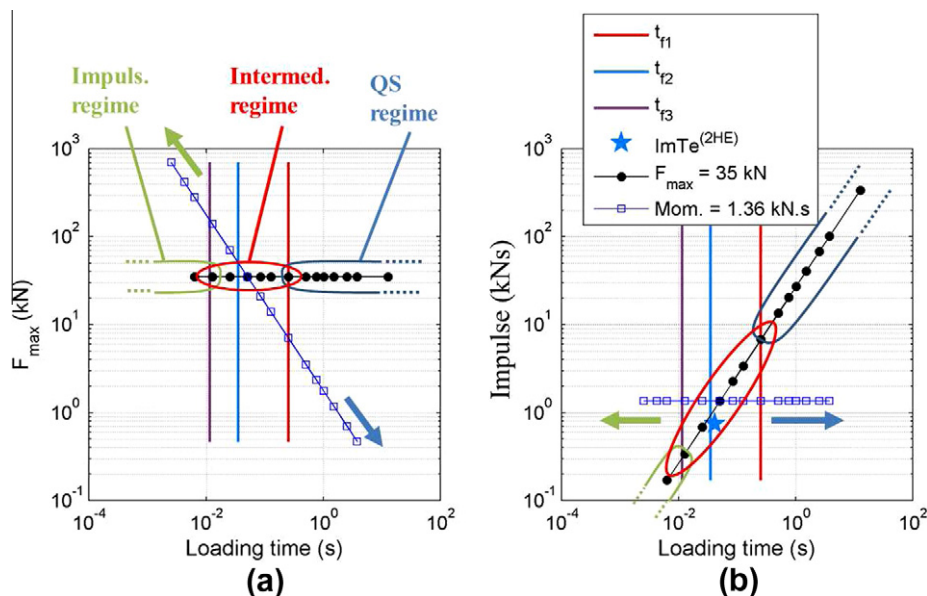


Fig. 12. Explored range of loading time for $F_{max} = 35 \text{ kN}$ (a) and $I = 1.36 \text{ kNs}$ (b). Identification of the stem response regimes ($ImTe^{(2)}$) in comparison to its natural periods (t_{f1} , t_{f2} and t_{f3}). The blue points (resp. the green points) correspond to a quasi-static (resp. impulsive) response of the stem ($t_c > 3 t_{f1}$), (resp. $t_c < t_{f1}/5$). The red points correspond to a transition regime. These time limits were deduced from the FE model. (For interpretation of the references to colour in this figure legend, the reader is referred to the web version of this article.)

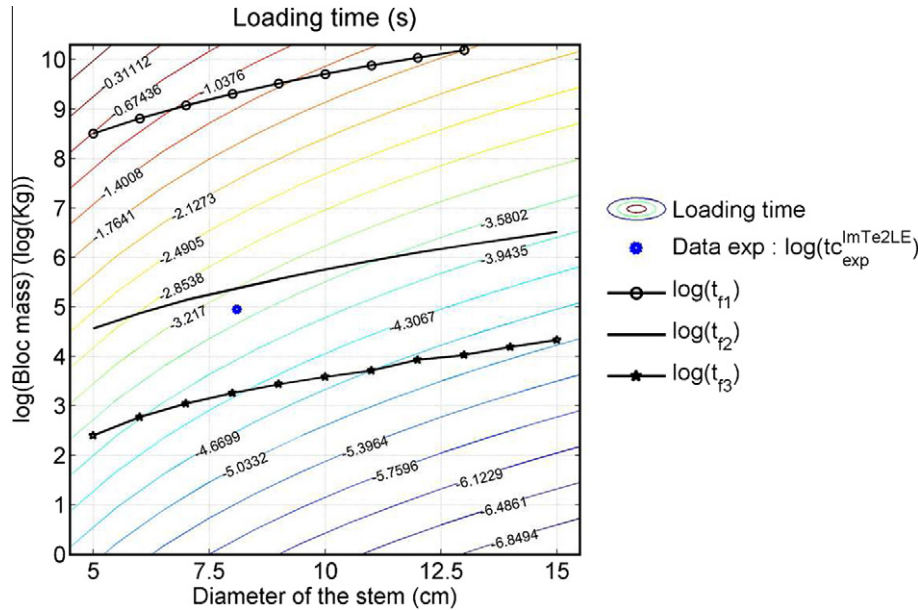


Fig. 13. Loading time estimation as a function of the block's mass and the stem's diameter. The three black curves represent the first three natural periods of the $ImTe^{(2)}$ stem. All the other features of the stem were kept constant. The blue point corresponds to the $ImTe^{(2HE)}$ experimental test.

The aim was to characterize the loading duration range corresponding to the transition from an impulsive to a quasi-static loading regime. If the maximum force is kept constant, this transition can be observed. Fig. 11a shows the maximum displacement at the top of the stem as a function of the loading time. Beyond $t_c = 1$ s, the displacements no longer depend on the loading time, which means the stem is subjected to a quasi-static loading. On the contrary, when the loading duration is short compared to the characteristic times of the structure (the first three periods of natural vibration are $t_{f1} = 0.25$ s, $t_{f2} = 0.028$ s and $t_{f3} = 0.012$ s), the impulse is also very small, implying a significant reduction in the displacements. However, high-frequency oscillations develop. Because the loading is applied very quickly, the response regime is impulsive. *In fine*, during the transition from one to regime another, the interaction between the block and the stem plays a very important role in the structure's overall kinematics, maximizing the displacements.

Fig. 11c shows the evolution of the maximum displacement as a function of the loading time when the impulse is kept constant. The higher the loading time is, the lower the displacements are. Actually, if the impulse is kept constant, when the loading time increases, the maximum force decreases, leading to lower displacement and a quasi-static regime. If the loading time decreases, the maximum displacement tends toward a limit whatever maximal force is applied (Fig. 11d), a typical response to an impulsive loading.

Fig. 12a–b summarizes the values tested for the loading times. As expected, the comparison of the loading time to the stem's natural periods predicts the stem's response regime.

Finally, an order of magnitude of the loading time can be proposed by Eq. 4, which can be used assuming an elastic behavior of the colliding bodies.

$$t_c^p = \sqrt{\frac{m_{iptor}}{k_{rot}}} h_{imp} \quad \text{with} \quad k_{rot} = \frac{E_{wood} \times I_{stem}}{L_{stem}} \quad (4)$$

where m_{iptor} (here $m_{iptor} = m_1 + \frac{4}{3}m_2$) is the impactor mass, E_{wood} the Young modulus of the wood, L_{stem} the stem's length, h_{imp} the impact height and $I_{stem} = \frac{\pi D_{stem}^4}{64}$ the inertia of the stem where D_{stem} is the stem's diameter. k_{rot} is the stem's rotational stiffness (i.e.,

$M_{fz} = k_{rot} \frac{d\theta}{dx}$ deduced from $EI \frac{d^2v}{dx^2} = M_{fz}$). The loading times measured were compared to the predicted times and the same order of magnitude was found (Table 2). For the $ImTe^{(2HE)}$ impact test, the loading time was underestimated because the stem rupture, which means that the stem is no longer elastic and the formula is no longer valid.

Eq. 4 expresses the loading time as a function of the block's mass and the stem's diameter. Fig. 13 compares the loading time to the natural periods of the $ImTe^{(2HE)}$ stems thus identifying the different regimes of the stem's response as a function of the stem's diameter and the impacting mass.

4. Conclusion

Dynamic tests (winching and impact tests) and a specific experimental setup were considered to analyze the impact between a rock and a small-diameter tree.

These tests allowed calibrating and validating a FE model for live stems under dynamic loadings. The FE model accounts for the wood's multifiber feature as well as the dissymmetry of the mechanical response under tensile and compressive regimes. The simulations showed a good agreement with the experimental measurements with a reduced computational cost. For European beech wood and for a stem diameter up to 81 mm, the ability of the FE model to predict the dynamic stem's response was demonstrated.

Live stem dynamics is strongly influenced by the impact force characteristics such as its maximal value, duration and qualitative time evolution during contact. To reproduce the stem's overall kinematics, the shape of the time evolution of the imposed force has to be considered carefully. We showed that imposing a double-peak-like shape of the contact force allows obtaining the same displacements observed in laboratory experiments.

Furthermore, attaching the stem to the support also has a huge influence on the overall response. Indeed, the cement crushing at the base of the stem modifies the rotational stiffness and thus partially controls the displacement field evolution and the energy transfers. The nature of the anchorage plays a very important role, underlining that the mechanical description of the root–earth system is needed for a relevant description of the dynamic response of *in situ* trees.

Parametrical studies have shown that the imposed force influences the stem's dynamic response. The relative mass and relative stiffness between the colliding bodies impose the dynamic regime under which the stem reacts. Three regimes exist (quasi-static/intermediate/impulsive). For a given impact situation, the stem's dynamic regime can be predicted based on the system's characteristic times (natural periods of free oscillation and contact duration).

The FE model presented can potentially provide essential information for the integration of the effect of trees in rockfall propagation models. Although the model proposed does not explicitly integrate either the interaction between the rock and the tree stem or the effect of the tree anchorage and the crown, important information can be gathered to properly describe the displacements of the tree stem for use in more complex models. This information is of specific interest for modeling the interaction between the rocks and small trees because, in this case, correct modeling of the stem's large displacements strongly influences energy transfers. Although the effects of small trees on the propagation of rocks has not yet been extensively studied (Ciabocco et al., 2009; Jancke et al., 2009), their integration into rockfall propagation models is even more important in practice. Coppice stands, mainly composed of a large number of small trees, are often neglected in the evaluation of forest protection effects whereas their contribution has been shown to be non-negligible (Jancke et al., 2009), especially since they are generally located in the bottom of slopes near the elements at risk.

Acknowledgments

This work has been partially supported by RNVOR (Research network on vulnerability of structures undergoing natural or technological hazards). The authors are very grateful to this scientific federation for its assistance in this project and particularly for the development of the experimental setup. Moreover, the support of the L.G.C.I.E. research laboratory at INSA Lyon, as well as the technical assistance, are gratefully acknowledged by the authors.

References

- Abrate, S., 2011. *Impact Engineering of Composite Structures*. Springer, Wien, New York.
- Adalian, C., Morlier, P., 2002. Wood model for the dynamic behaviour of wood in multiaxial compression. *Holz als Roh- und Werkstoff* 60, 433–439.
- Sdt ASTM., 2010. *Astm d6110 – 10 standard test method for determining the charpy impact resistance of notched specimens of plastics*. In: American Society for Testing and Materials, ASTM International.
- Biggs, J., 1964. *Introduction to Structural Dynamics*. McGraw-Hill.
- Cameron, E., Peloso, G., 2009. Choosing a rockfall barrier with the precautionary principle: a quantitative approach. *Environ. Earth Sci.* 59, 161–172.
- Christoforou, A., Yigit, A., 1998. Effect of flexibility on low velocity impact response. *J. Sound Vibr.* 217 (2), 563–578.
- Ciabocco, G., Boccia, L., Ripa, M.N., 2009. Energy dissipation of rockfalls by coppice structures. *Nat. Hazards Earth Syst. Sci.* 9 (3), 993–1001.
- DaSilva, A., Kyriakides, S., 2007. Compressive response and failure of balsa wood. *Int. J. Solids Struct.* 44, 8685–8717.
- Dorren, L., 2006. Real-size experiments and 3d simulation of rockfall on forested and non-forested slopes. *Nat. Hazards Earth Syst. Sci.* 6, 145–153.
- Goldsmith, W., 1960. *Impact – The theory and Physical Behaviour of Colliding Solids*. Dover Pub. Inc.
- Guedes, J., Pegon, P., Pinto, A., 1994. A fibre timoshenko beam element in castem 2000. *Note technique 1.94.31*, CEA Saclay, pp. 8.
- Hu, X., Tao, W., Guo, Y., 2008. Using fem to predict tree motion in a wind field. *J. Zhejiang Univ. Sci. A* 9 (7), 907–915.
- Jancke, O., Dorren, L.K.A., Berger, F., Fuhr, M., Kohl, M., 2009. Implications of coppice stand characteristics on the rockfall protection function. *For. Ecol. Manage.* 259 (1), 124–131.
- Jonsson, M., 2007. *Energy absorption of trees in a rockfall protection forest*. PhD thesis, Swiss federal institute of technology of Zurich.
- Lundstrom, T., Jonsson, M., Kalberer, M., 2007. The root-soil system of norway spruce subjected to turning moment: resistance as a function of rotation. *Plant Soil* 300, 35–49.
- Macklerle, J., 2005. Finite element analyses in wood research: a bibliography. *Wood Sci. Technol.* 39, 579–600 (ISSN: 0043-7719).
- Mindess, S., Madsen, B., 1986. The fracture of wood under impact loading. *Mater. Struct.* 19, 49–53 (ISSN: 1359-5997).
- Mittal, R., 1989. A closed form solution for the response of a long elastic beam to dynamic loading. *Ingenieur-Archiv*, 41–50.
- Miyamoto, A., King, M., Fuji, M., 1991. Integrated analytical procedure for concrete slabs under impact loads. *J. Struct. Eng.* 120 (6), 1685–1702.
- Neumann, M., Herter, J., Droste, B., Hartwig, S., 2011. Compressive behaviour of axially loaded spruce wood under large deformations at different strain rates. *Eur. J. Wood Wood Prod.* 69, 345–357.
- Oudjene, M., Khelifa, M., 2009. Elasto-plastic constitutive law for wood behaviour under compressive loadings. *Constr. Build. Mater.* 23, 3359–3366.
- Pashah, S., Massenzio, M., Jacquelin, E., 2008. Prediction of structural response for low velocity impact. *Int. J. Impact Eng.* 35, 119–132.
- Perret, S., Dolf, F., Kienholz, H., 2004. Rockfalls into forests: Analysis and simulation of rockfall trajectories – considerations with respect to mountainous forests in switzerland. *Landslides* 1, 123–130.
- Quetel, C., 2005. *Approche multi-échelle du comportement mécanique d'un arbre soumis à l'impact d'un bloc rocheux*. Ph.D. thesis, Ecole Centrale de Lyon.
- Reid, S., Peng, C., 1997. Dynamic uniaxial crushing of wood. *Int. J. Impact Eng.* 19 (5–6), 531–570.
- Risbrudt, C., Ritter, M., Wegner, T., 2010. *Wood Handbook - Wood as an engineering material*. Forest Products Laboratory.
- Ruel, J., Achim, A., Herrera, R., Cloutier, A., 2010. Relating mechanical strength at the stem level to values obtained from defect-free wood samples. *Trees* 24, 1127–1135.
- Salmi, A., Salminen, L., Engberg, B., Bjorkqvist, T., Haeggstrom, E., 2012. Repetitive impact loading causes local plastic deformation in wood. *J. Appl. Phys.* 111, 024901.
- Schwieger, H., 1970. Central deflection of a transversely struck beam. *Exp. Mech.* 10 (4), 166–169.
- Sellier, D., Fourcaud, T., Lac, P., 2006. A finite element model for investigating effects of aerial architecture on tree oscillations. *Tree Physiol.* 26, 799–806.
- Stokes, A., Salin, F., Kokutse, A., Berthier, S., Jeannin, H., Mochan, S., Dorren, L., Kokutse, N., Ghani, M., Fourcaud, T., 2005. Mechanical resistance of different tree species to rockfall in the french alps. *Plant Soil* 278, 107–117.
- Stronge, W., 2000. *Impact Mechanics*. Cambridge Univ Press.
- Timoshenko, S., Woinowsky-Krieger, S., 1959. *Theory of Plates and Shells*. McGraw-Hill.
- Trouy-Triboulot, M., Triboulot, P., 2008. *Structure et caractéristiques*. Technical report, Techniques de l'ingénieur.
- Urata, T., Shibuya, M., Koizumi, A., Torita, H., Cha, J., 2012. Both stem and crown mass affect tree resistance to uprooting. *J. For. Res.* 17, 65–71.
- Volkwein, A., Schellenberg, K., Labiouse, V., Agliardi, F., Berger, F., Bourrier, F., Dorren, L., Gerber, W., Jaboyedoff, M., 2011. Rockfall characterisation and structural protection – a review. *Nat. Hazard Earth Syst. Sci.* 11, 2617–2651.
- Wilson, J., 2004. Segmented impact fracture of toppling truncated cones and tall trees. *Int. J. Impact Eng.* 30, 351–365.